Longitudinal chirality, enhanced nonreciprocity, and nanoscale planar one-way plasmonic guiding

Y. Mazor and Ben Z. Steinberg*
School of Electrical Engineering, Tel Aviv University, Ramat-Aviv, Tel-Aviv 69978, Israel
(Received 24 January 2012; revised manuscript received 26 June 2012; published 16 July 2012)

When a linear chain of plasmonic nanoparticles is exposed to a transverse dc magnetic field, the chain modes are elliptically polarized in a single plane parallel to the chain axis; hence, a new chain mode of longitudinal plasmon rotation is created. If, in addition, the chain geometry possesses longitudinal rotation, e.g., by using ellipsoidal particles that rotate in the same plane as the plasmon rotation, strong nonreciprocity is created. The structure possesses a new kind of chirality—longitudinal chirality—and supports one-way guiding. Since all particles rotate in the same plane, the geometry is planar and can be fabricated by printing leaflike patches on a single plane. Furthermore, the magnetic field is significantly weaker than in previously reported one-way guiding structures. These properties are examined for ideal (lossless) and lossy chains.

DOI: 10.1103/PhysRevB.86.045120 PACS number(s): 41.20.Jb, 42.70.Qs, 42.82.Et, 78.67.Bf

I. INTRODUCTION

Linear chains of identical and equally spaced nanoparticles were explored in a number of studies.[1–4] They support optical modes with relatively low attenuation and with no radiation to the free space if the interparticle distance is smaller than the free space wavelength λ, and then the modes can be much narrower than λ, hence the name "subdiffraction chains" (SDC). SDCs were proposed as waveguides, junctions, and couplers.[1–6]

Recently, SDCs were suggested as candidates for one-way guiding.[7] The physics there is based on creating an interplay of two types of rotations: geometrical chirality and Faraday rotation (caused by longitudinal magnetization). This interplay strongly enhances nonreciprocity and eventually leads to one-way guiding. The attractive features in Ref. 7 are the three-dimensional (3D) nanoscale dimensions and the fact that the magnetic field bias is an order of magnitude weaker compared to some alternative structures.[8] However, its chiral geometry is difficult to fabricate. Other works on one-way guiding employ periodic structures of nonreciprocal material operating around their Bragg point, thus requiring relatively large structures.[9]

Here we suggest an alternative type of SDC for one-way optical guiding. The structure is planar in nature, so it can be fabricated by relatively simple printing procedures of leaflike patches on a single plane. Moreover, it requires a magnetization field that is significantly weaker than that in Refs. 7 and 8. The underlying physics and geometry are described in Figs. 1 and 2. A conventional SDC of spherical plasmonic particles supports three independent electric dipole modes: one with longitudinal polarization p_z and two degenerate modes with transverse and mutually orthogonal polarizations p_x, p_y.[4] If this SDC is exposed to transverse magnetization, as shown in Fig. 1, the p_y mode is unaffected, but $\boldsymbol{B}_0 = \hat{\boldsymbol{y}} B_0$ couples p_x and p_z. This coupling creates two new modes of elliptical polarizations in the x,z plane, with two new dispersion curves (see the analysis below). At any operation frequency, one wave propagates in the direction of rotation ("paddles" forward and "rides" forward) and the second propagates counter to the rotation (paddles forward and rides backward). Hence, these new SDC modes are nonreciprocal. However, their dispersion is still reciprocal (i.e., even in β). The route to enhanced nonreciprocity and one-way guiding is to create an interplay of *two-type rotations*. Hence, we add a *longitudinal chirality*: we replace the spheres by ellipsoids, rotated in the same plane of the elliptical polarization, i.e., in the x,z plane, as shown in Fig. 2. The rotation step is $\Delta\theta$. As we show below, this chain indeed supports one-way guiding. It is periodic only for rational $\Delta\theta/\pi$. If $\Delta\theta/\pi = n/m$ and m,n are coprime, then the period consists of m particles. Unlike the spiral structure in Ref. 7, if this ratio is irrational then *there is no coordinate transformation under which the chain becomes periodic*.

Below we use the discrete dipole approximation (DDA) and polarizability theory. These are standard tools in SDC analysis.[3–6] They hold when the particle radius a and interparticle distance d satisfy $a \ll \lambda$ and $a \ll d$, but studies show good accuracy even for $d = 3a$.[10]

II. FORMULATION

If a small particle with polarizability $\boldsymbol{\alpha}$ is subject to an electric field whose local value in the *absence of the particle* is $\boldsymbol{E}^L$, its response is described by the electric dipole $\boldsymbol{p} = \boldsymbol{\alpha}\boldsymbol{E}^L$. The dynamic tensor polarizability of a general ellipsoid whose principal axes are aligned with the x,y,z axes, made of an anisotropic material with electric susceptibility $\boldsymbol{\chi}$, is obtained via

$$\epsilon_0 \boldsymbol{\alpha}^{-1} = V^{-1}(\boldsymbol{\chi}^{-1} + \mathbf{L}) - \frac{ik^3}{6\pi}\mathbf{I}. \tag{1}$$

Here k is the vacuum wave number, $\mathbf{I}$ is the 3×3 identity matrix, and the imaginary term $ik^3(6\pi)^{-1}\mathbf{I}$ represents radiation loss. $V = 4\pi a_x a_y a_z/3$ is the ellipsoid volume with a_x, a_y, a_z its principal semiaxes, and $\mathbf{L} = \mathrm{diag}(N_x, N_y, N_z)$ is the depolarization matrix whose entries are obtained from a_x, a_y, a_z by elliptic integrals and satisfy $\sum_u N_u = 1$.[11] Under the Drude model and magnetization $\boldsymbol{B}_0 = \hat{\boldsymbol{y}} B_0$, $\boldsymbol{\chi}$ is[12]

$$\boldsymbol{\chi} = \frac{-\bar{\omega}^{-2}}{(\bar{\omega} + i\sigma)^2 - \bar{\omega}_b^2} \begin{pmatrix} \bar{\chi}_{xx} & 0 & \bar{\chi}_{xz} \\ 0 & \bar{\chi}_{yy} & 0 \\ -\bar{\chi}_{xz} & 0 & \bar{\chi}_{zz} \end{pmatrix}, \tag{2}$$

with $\bar{\chi}_{xx} = \bar{\chi}_{zz} = \bar{\omega}^2 + i\sigma\bar{\omega}$, $\bar{\chi}_{yy} = \bar{\chi}_{xx} - \bar{\omega}\bar{\omega}_b^2/(\bar{\omega} + i\sigma)$, and $\bar{\chi}_{xz} = i\bar{\omega}\bar{\omega}_b$, and where $\bar{\omega} = \omega/\omega_p$, $\bar{\omega}_b = \omega_b/\omega_p$, and where ω_p and $\omega_b = -q_e B_0/m_e$ are the plasma and cyclotron

 ©2012 American Physical Society

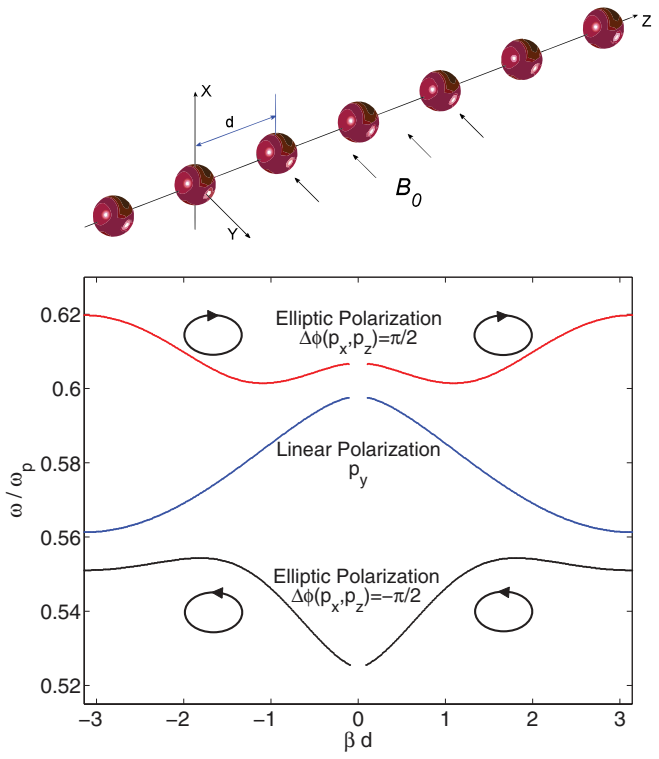

FIG. 1. (Color online) Top: a chain of spherical plasmonic particles with transverse magnetization. This chain supports modes with *longitudinal* rotation. Bottom: supported mode dispersion.

frequencies. $\sigma = (\tau\omega_p)^{-1}$ represents loss, where τ is the dissipation time constant. Equations (1) and (2) fully describe the ellipsoid at the origin. The nth particle polarizability, $\boldsymbol{\alpha}_n$, is given by the $n\Delta\theta$ *longitudinal rotation* (about $\hat{\mathbf{y}}$),

$$\boldsymbol{\alpha}_n = \mathbf{T}^{\ell}_{-n}\boldsymbol{\alpha}\mathbf{T}^{\ell}_{n}, \tag{3}$$

where the nonzero entries of $\mathbf{T}^{\ell}_n$ are $t_{11} = t_{33} = \cos n\Delta\theta, t_{22} = 1$, and $t_{13} = -t_{31} = \sin n\Delta\theta$. The electric field at $(0,0,z)$ due to a short dipole $\boldsymbol{p}$ at $(0,0,z')$ is given by the matrix relation $\boldsymbol{E}(z) = \epsilon_0^{-1}\mathbf{A}(z-z')\,\boldsymbol{p}$, where

$$\mathbf{A}(z) = \frac{e^{ik|z|}}{4\pi\,|z|}\left[k^2\mathbf{A}_1 + \left(\frac{1}{z^2} - \frac{ik}{|z|}\right)\mathbf{A}_2\right]. \tag{4}$$

Here $\mathbf{A}_1 = \mathrm{diag}(1,1,0)$ and $\mathbf{A}_2 = \mathrm{diag}(-1,-1,2)$. We express now the local exciting field of the mth particle in the chain as a sum of contributions from all its neighbor dipoles, and we apply $\boldsymbol{\alpha}_m$. The result relates the mth dipole excitation

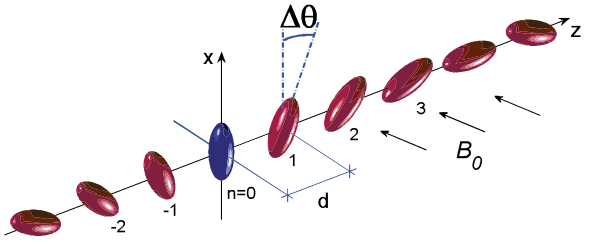

FIG. 2. (Color online) A chain of plasmonic prolate ellipsoids with transverse magnetization and *longitudinal chirality*. This chain supports one-way optical guiding.

$\boldsymbol{p}_m$ to its neighbors,

$$\boldsymbol{p}_m = \epsilon_0^{-1}\boldsymbol{\alpha}_m \sum_{n,\,n\neq m} \mathbf{A}[(m-n)d]\;\boldsymbol{p}_n. \tag{5}$$

This equation is not shift-invariant. Furthermore, since $\mathbf{T}^{\ell}_n$ is a rotation about $\hat{\mathbf{y}}$ and not about the longitudinal axis $\hat{\mathbf{z}}$, it does not commute with the propagator $\mathbf{A}$ so the mathematical transformation used in Ref. 7 cannot be applied. However, we set $\Delta\theta/\pi = N/M$ rational, hence the period $D = Md$ consists of M particles with polarizabilities $\boldsymbol{\alpha}_0, \boldsymbol{\alpha}_1, \ldots, \boldsymbol{\alpha}_{M-1}$ as in Eq. (3) and $\boldsymbol{\alpha}_{m+lM} = \boldsymbol{\alpha}_m\ \forall$ integer l. Then by periodicity

$$\boldsymbol{p}_{n+lM} = \boldsymbol{p}_n e^{i\beta lMd}, \tag{6}$$

and the chain modes are determined from the M vectors of the reference period $\boldsymbol{p}_0, \ldots, \boldsymbol{p}_{M-1}$. We substitute this solution into Eq. (5). For each m within a period, we decompose the infinite sum into a sum $\boldsymbol{S}_0$ of contributions from identical particles ($n = m + lM, l \neq 0$) and a set of summations $\boldsymbol{S}_{m-n'}$ of contributions from the rest ($n = n' + lM, n' \neq m$). The result is the $3M \times 3M$ matrix equation

$$\left(\epsilon_0\boldsymbol{\alpha}_m^{-1} - \boldsymbol{S}_0\right)\boldsymbol{p}_m - \sum_{n=0,n\neq m}^{M-1} \boldsymbol{S}_{m-n}\,\boldsymbol{p}_n = 0, \tag{7}$$

with $m = 0, \ldots, M-1$, and where

$$\boldsymbol{S}_q = \begin{cases} \sum_{l\neq 0} \boldsymbol{A}(lD)e^{i\beta lD}, & q = 0, \\ \sum_l \boldsymbol{A}(qd - lD)e^{i\beta lD}, & 1 \leqslant |q| < M. \end{cases} \tag{8}$$

The modes are obtained by looking for $\omega(\beta)$ at which the Eq. (7) determinant vanishes. The vectors that span the corresponding null space are $\boldsymbol{p}_0, \ldots, \boldsymbol{p}_{M-1}$, which, with Eq. (6), describe the entire chain excitation.

Note that the series for $\boldsymbol{S}_q$ above converge poorly. However, they can be cast in terms of the polylogarithm functions Li_s, for which efficient summation formulas exist (see Refs. 4 and 13 and the Appendix). First observe that the matrix $\boldsymbol{S}_0$ is identical to that obtained in conventional chains with $d = D$. Hence[4]

$$\boldsymbol{S}_0 = \frac{k^3}{4\pi}\sum_{s=1}^{3} u_s\, f_s(kD,\beta D)\boldsymbol{A}_s, \tag{9}$$

where $(u_1,u_2,u_3) = (1,-i,1), \boldsymbol{A}_3 = \boldsymbol{A}_2$, and

$$f_s(x,y) = x^{-s}[\mathrm{Li}_s(e^{ix+iy}) + \mathrm{Li}_s(e^{ix-iy})], \tag{10}$$

where $\mathrm{Li}_s(z) \equiv \sum_{n=1}^{\infty} \frac{z^n}{n^s}$ is the sth-order polylogarithm function. To write $\boldsymbol{S}_q$ in terms of Li_s, note that all sums in $\boldsymbol{S}_q$ have the general form

$$\zeta = \sum_{l=0}^{\infty} \frac{(e^{i\xi})^{lM+q}}{(lM+q)^s} = \sum_{n=1}^{\infty} \frac{(e^{i\xi})^n}{n^s} a_n(q), \tag{11}$$

where $a_n(q) = a_{n+M}(q)$ is an M-periodic sequence with $a_n(q) = 0$ for $1 \leqslant n \neq q \leqslant M$, and $a_q(q) = 1$. But $Ma_n(q) = \sum_{r=0}^{M-1} e^{i2\pi r(n-q)/M}$, hence

$$\zeta = M^{-1}\sum_{r=0}^{M-1} e^{-i2\pi rq/M}\mathrm{Li}_s(e^{i\xi+i2\pi r/M}). \tag{12}$$

Following the standard steps leading from Eq. (8) to Eq. (9) and using Eq. (12), we get for $\boldsymbol{S}_q, 1 \leqslant |q| < M$, the same

expression as in Eq. (9) but with f_s replaced by $h_s(kd,\beta d;q)$,

$$h_s(x,y;q)=\frac{e^{iyq}}{M}\sum_{r=0}^{M-1}e^{-i2\pi\frac{rq}{M}}f_s\left(x,y-\frac{2\pi r}{M}\right). \quad (13)$$

III. EXAMPLES

We turn to study the structure. First, we examine a transversely magnetized chain of *spherical* particles of radius a. It is a special case of Eq. (7) with the sum over $\boldsymbol{S}_q, q\neq 0$ dropped, with $M=1(D=d)$, $\Delta\theta=0$, and $\boldsymbol{\alpha}_0=\boldsymbol{\alpha}$ given by Eqs. (1) and (2) with all depolarization factors set to 1/3. The chain dispersion is obtained by $\det(\epsilon_0\boldsymbol{\alpha}^{-1}-\boldsymbol{S}_0)=0$. For a lossless chain, this can be satisfied only if $\mathrm{Im}[\mathrm{diag}(\boldsymbol{S}_0)]=-k^3/(6\pi)$. Also, the first and third rows of Eq. (7) are now linearly dependent and read

$$\{\bar{\omega}^2-1/3+V[(\boldsymbol{S}_0)_{11}+ik^3/(6\pi)]\}p_x=i\bar{\omega}\bar{\omega}_b p_z. \quad (14)$$

However, as discussed above, the term in the square brackets must be real. Hence there is a phase difference of $\pm\pi/2$ between p_z and p_x if $\bar{\omega}_b\neq 0$. This implies that the chain modes are elliptically polarized in the (x,z) plane.

The chain dispersion for $d=3a=\lambda_p/30$ and no loss was calculated numerically and is shown in Fig. 1. We have applied a relatively strong magnetization of $\omega_b=0.05\omega_p$ in order to observe the features clearly (the one-way property shown below is obtained at much weaker magnetizations). The $\hat{\boldsymbol{y}}$-polarized mode is identical to that of a conventional chain. Two additional modes of elliptic polarization in the x,z plane exist in the chain. When observed from $y>0$, one rotates clockwise [shown by the upper (red) curve] and the second rotates counterclockwise [shown by the lower (black) curve]. This elliptic polarization is only due to the transverse magnetization. It is mathematically evident from the $\pm\pi/2$ phase difference between the $\hat{\boldsymbol{x}}$ and $\hat{\boldsymbol{z}}$ components we have observed in the solutions for $\boldsymbol{p}_0$, as seen in Eq. (14). All dispersion curves are even in β, permitting propagation in both $+z$ and $-z$ directions. Also all dispersion curves possess the light-line gap clearly seen in the center. However, the light-line dispersion branches that run parallel to the light-line cone $\beta=\omega/c$ and that are associated with transverse polarization in conventional chains[4,14] represent modes that are practically not excited[14] in the elliptically polarized curves (red and black). To avoid cluttering up the figure, they are not shown here.

Next, we add *longitudinal chirality*. We replace the spheres by prolate ellipsoids with semiaxis $a_x=\lambda_p/90$, an axis ratio of $a_y=a_z=0.9a_x$ (nearly spheres), and we add longitudinal chirality with $\Delta\theta=\pi/3$ (hence the chain period is $D=3d=\lambda_p/10$). Figure 3 shows the results for the relatively weak magnetization of $\omega_b=0.005\omega_p$. Due to the added chirality, the upper (red) dispersion curve of Fig. 1 that corresponds to elliptical polarization with clockwise longitudinal rotation splits into three branches, as shown in Fig. 3(a), and shifts the light-line gap rightward. Hence symmetry is broken and one-way guiding is supported at frequencies within the shifted gap, as shown in Fig. 3(b). Finally, in Fig. 3(c) we show the normalized response $|\boldsymbol{p}_n|/|\boldsymbol{p}_0|$ of a finite chain of $N=600$ particles with the parameters above, for a unit amplitude excitation of the central particle (at the origin), at the selected

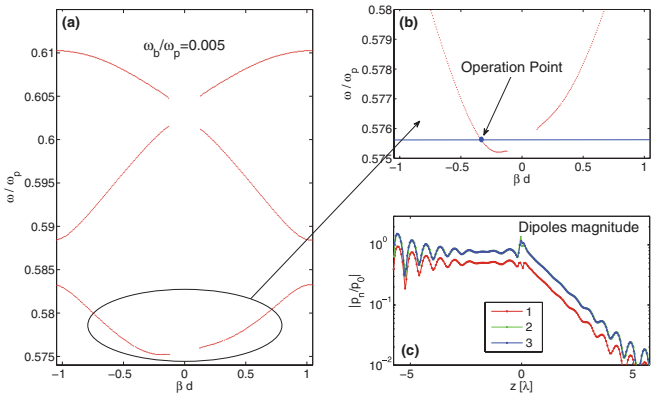

FIG. 3. (Color online) One-way guiding in the upper band. (a) Dispersion curves. The gap in Fig. 1 is shifted rightward by the longitudinal chirality. (b) Frequency selection for one-way guiding. (c) Chain response.

frequency. This response is obtained by solving Eq. (5) for a finite number of particles, with only the central particle forced to oscillate at the aforementioned frequency [hence it is a matrix equation of $3(N-1)$ unknowns]. The three curves in Fig. 3(c) correspond to the three particles within each period. One-way guiding is clearly observed (note the logarithmic scale). Essentially the same picture holds for the lower (black) dispersion curve of Fig. 1, which corresponds to elliptical polarization with counterclockwise longitudinal rotation when the above longitudinal chirality is added to the structure. This is shown in Fig. 4.

We note that these results are obtained with a very slight breach of spherical symmetry ($a_z=0.9a_x$). This low ellipticity is sufficient to create one-way guiding if $\boldsymbol{B}_0=\hat{\boldsymbol{y}}B_0$ is present. In addition, B_0 is considerably weaker than that required in previous studies on one-way plasmonic waveguides.

Next, we study chains with loss. Since a *real* dispersion $\omega(\beta)$ does not exist, we have solved Eq. (5) for a finite chain with $N=250$ and for the same geometrical parameters $(\Delta\theta,d)$ as in the lossless example of Fig. 4. The operation frequency ω and axes ratio $r=a_z/a_x$ were chosen by scanning over the neighborhoods of ω,r for which the corresponding lossless chain possesses a one-way property. The results are shown in Fig. 5. Figure 5(a) shows the chain response for loss parameter $\sigma=(\tau\omega_p)^{-1}=8.2\times10^{-4}$ corresponding

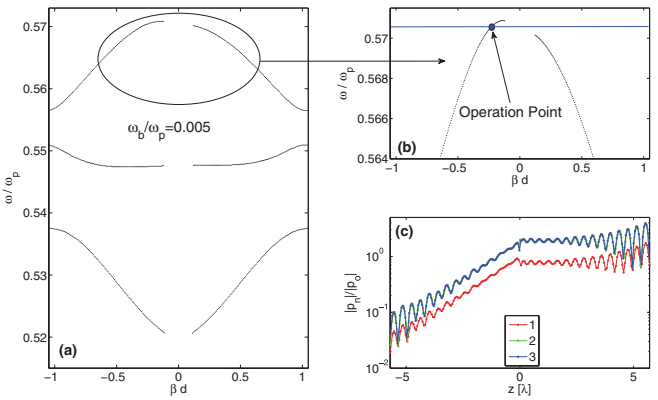

FIG. 4. (Color online) One-way guiding in the lower band.

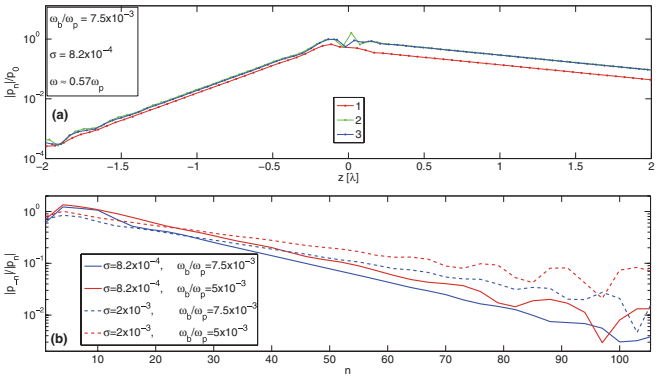

FIG. 5. (Color online) One-way guiding in a lossy chain. (a) Chain response. (b) Isolation ratio.

to palladium (Pd)[15] and the magnetization of $\omega_b = 7.5 \times 10^{-3}\omega_p$. It is obtained with $\omega \approx 0.57\omega_p$ and $r = 0.92$. For a clear assessment of the one-way property as a function of magnetization and loss, we plot in Fig. 5(b) the "isolation ratio" $|\boldsymbol{p}_{-n}|/|\boldsymbol{p}_n|$ versus n for various values of loss and magnetization. Again, one-way guiding is evident.

In the examples above, the particles are nearly spheres. These examples are important from the theoretical/physical point of view. They show that by using our approach of two-type rotation interplay, a very slight breach of symmetry is sufficient to create a profound nonreciprocity and one-way guiding. However, from a practical point of view, structure *flatness* is at least as important because it opens the way to employing planar fabrication technologies. To demonstrate this option, we have simulated a chain with the following properties. The axis ratio is $a_x : a_y : a_z = 1 : 0.1 : 0.75$, hence the particle's size in the $\hat{\boldsymbol{y}}$ direction is an order of magnitude smaller than its dimensions in the x,z plane. Since the longitudinal chirality is obtained by rotating the particles about their y axis, it follows that the entire structure is practically flat and lies in the x,z plane. Other geometrical parameters are as before, with a magnetization level of $\omega_b = 0.0075\omega_p$. A strong one-way property exists and it is shown in Fig. 6.

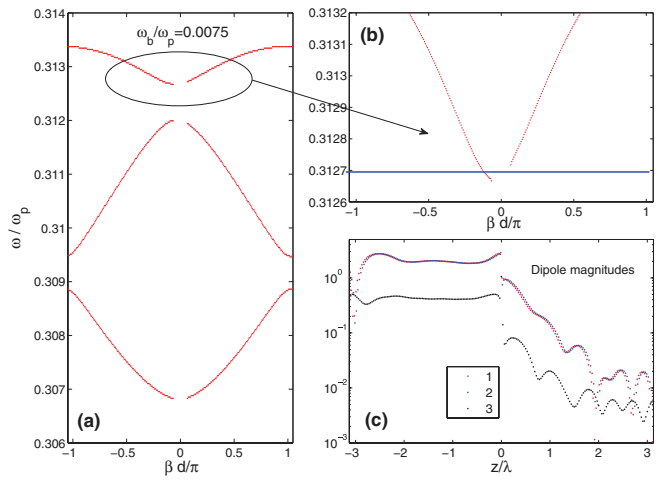

FIG. 6. (Color online) The same as Fig. 3 but for flat geometry with $a_x : a_y : a_z = 1 : 0.1 : 0.75$.

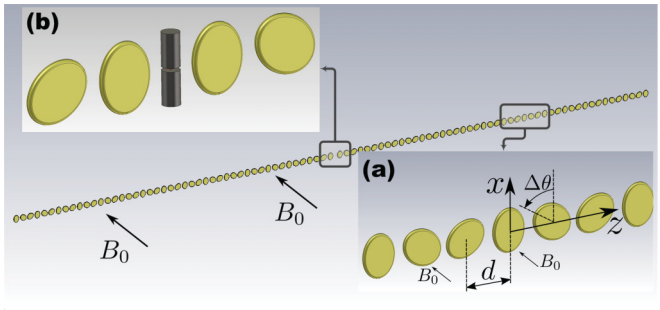

FIG. 7. (Color online) A flat chain geometry for one-way guiding. (a) Geometry details. (b) Excitation by a short dipole located in between two identical chains.

Finally, we verify our approach via a full-wave numerical solutions using the CST software package[16] for the flat structure shown in Fig. 7. The particles are disks of 2.5 nm thickness and of elliptical shape in the x,z plane with long and short diameters of 25 and 20 nm, respectively. The interparticle distance is $d = 27.5$ nm. The longitudinal chirality angle is $\Delta\theta = -60^\circ$. The particles' material plasma frequency ω_p and loss parameter τ^{-1} are $2\pi \times 2000$ THz and 2 THz, respectively (corresponding to Ag). Due to a limited availability of computing power and memory resources, we can apply the full-wave solution to chains of about 100 particles or less. Hence our chain consists of 92 particles that create two *identical* chains of 46 particles each, one chain on each side of a short dipole antenna that serves as a local source—see Fig. 7(b). Since this geometry should show significant one-way guiding within a distance of 46 particles only (instead of within hundreds of particles used to obtain the results of Fig. 5), we need to apply stronger magnetization. Hence we use $\omega_b = 0.03\omega_p$. We have used the DDA for a first estimate of the chain operation parameters, and then we used the CST to search more accurately around the initial guess and to get full-wave solutions. The full-wave-based chain response as a function of frequency is shown in Fig. 8. One-way

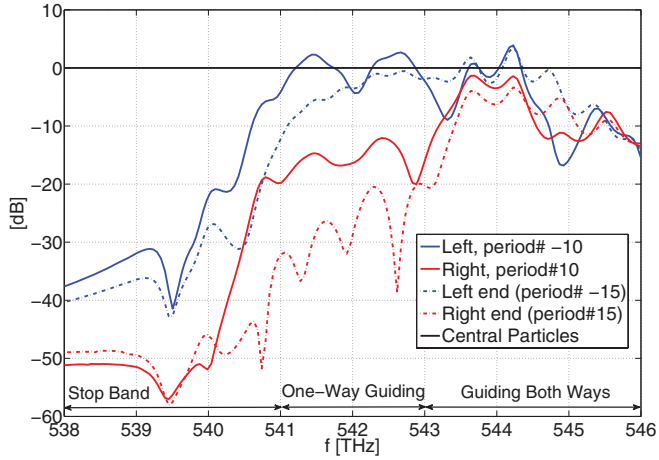

FIG. 8. (Color online) E-fields just above the upright particle in periods ±10 and ±15, obtained by full-wave solution of the chain shown in Fig. 7. For each frequency, the values are normalized to the field above the upright particle adjacent to the dipole from the left, shown in Fig. 7(b).

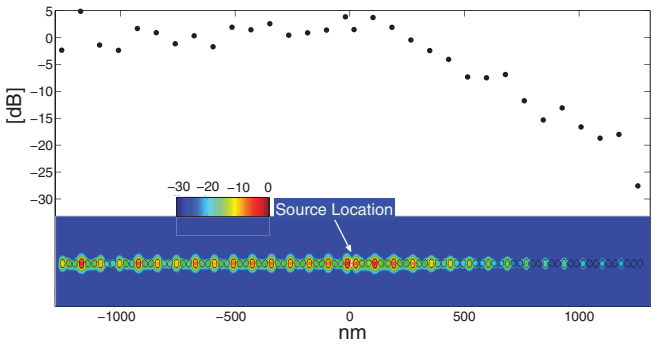

FIG. 9. (Color online) Full-wave solution for the E-field in the $y = 0$ plane, at 542 THz. Normalized fields in the center of each upright particle are shown on top.

behavior can be clearly observed within the frequency band of 541–543 THz. The ratio between the chain excitation on the left and right side of the chain—the isolation ratio—is on the order of 20 dB. Finally, Fig. 9 shows the E-field in the $y = 0$ plane at the central frequency of the one-way band, 542 THz.

Note that in this frequency, $\lambda \approx 0.55\ \mu$m. Hence a significant one-way behavior is clearly observed over distances of $O(\lambda)$.

IV. CONCLUSION

When an interplay of two-type rotations is supported in a guiding structure, strong nonreciprocity and one-way guiding are created.[7] In this work, a geometry possessing longitudinal chirality in subdiffraction particle chains is proposed. When combined with transverse magnetization, the resulting elliptical rotation of the chain dipole modes and the geometrical rotation (longitudinal chirality) provide the two-type rotation that leads to strong nonreciprocity and one-way guiding. The required magnetization is considerably weaker than in previously reported studies. This one-way chain can be fabricated by thin-layer printing of leaflike flakes of thin metals. Since single-atom layers of graphene may behave like thin metal flakes with controllable properties, exhibiting SPP-like behavior with very low loss,[17] the present work may offer a basic scheme for one-way guiding on a graphene layer. This is a subject of ongoing research.

ACKNOWLEDGMENTS

This research was supported by the Israel Science Foundation (Grant No. 1503/10).

APPENDIX: EVALUATION OF $\mathrm{Li}_s(e^{i\theta})$

$\mathrm{Li}_s(e^{ix})$ for real x can be expressed as finite sums of Clausen integrals.[13,18] The latter can be computed using series that converge much faster than the algebraic convergence of the formal definition in Eq. (8). Note that $\mathrm{Li}_1(z) = -\ln(1-z)$. Furthermore, from Eq. (8) it follows that

$$\mathrm{Li}_{s+1}(z) = \int_0^z t^{-1}\mathrm{Li}_s(t)dt. \tag{A1}$$

Collecting the Clausen integral components that constitute our Li_s and rearranging, we obtain for $s = 2$ and $|x| \leqslant \pi$,

$$\mathrm{Li}_2(e^{ix}) = \frac{\pi^2}{6} - \frac{x}{4}(2\pi - x) - i\left[x\ln x - x - \frac{1}{2}\sum_{n=1}^{\infty}\frac{B_{2n}x^{2n+1}}{n(2n+1)(2n)!}\right], \tag{A2}$$

where B_{2n} are the absolute value of the Bernoulli numbers. With terms up to $n = 5$ in the series above, the relative error for $x = \pi$ is on the order of 10^{-5}. From the integral relation Eq. (A1), we obtain

$$\mathrm{Li}_3(e^{ix}) = \zeta(3) + \frac{x^2}{2}(\ln x - 3/2) - \frac{1}{4}\sum_{n=1}^{\infty}\frac{B_{2n}x^{2n+2}}{n(n+1)(2n+1)(2n)!} + i\left(\frac{\pi^2 x}{6} - \frac{\pi x^2}{4} + \frac{x^3}{12}\right), \tag{A3}$$

where $\zeta(3) \approx 1.202\,056\,9$. Higher-order polylogarithm functions are not needed in the present work.

*Author to whom all correspondence should be addressed: steinber@eng.tau.ac.il

[1] M. Quinten, A. Leitner, J. R. Krenn, and F. R. Aussenegg, Opt. Lett. **23**, 1331 (1998).
[2] S. A. Tretyakov and A. J. Viitanen, Electr. Eng. **82**, 353 (2000).
[3] M. L. Brongersma, J. W. Hartman, and H. A. Atwater, Phys. Rev. B **62**, R16356 (2000).
[4] A. Alu and N. Engheta, Phys. Rev. B **74**, 205436 (2006).
[5] D. V. Orden, Y. Fainman, and V. Lomakin, Opt. Lett. **34**, 422 (2009).
[6] D. V. Orden, Y. Fainman, and V. Lomakin, Opt. Lett. **35**, 2579 (2010).
[7] Y. Hadad and B. Z. Steinberg, Phys. Rev. Lett. **105**, 233904 (2010).
[8] Z. Yu, G. Veronis, Z. Wang, and S. Fan, Phys. Rev. Lett. **100**, 023902 (2008).
[9] Z. Yu, Z. Wang, and S. Fan, Appl. Phys. Lett. **90**, 121133 (2007).
[10] S. A. Maier, P. G. Kik, and H. A. Atwater, Phys. Rev. B **67**, 205402 (2003).
[11] A. H. Sihvola, *Electromagnetic Mixing Formulas and Applications*, Electromagnetic Waves Series (IEE, London, 1999).
[12] J. D. Jackson, *Classical Electrodynamics*, 3rd ed. (Wiley, 1999).
[13] L. Lewin, *Polylogarithms and Associated Functions* (Elsevier, New York, 1981).
[14] Y. Hadad and B. Z. Steinberg, Phys. Rev. B **84**, 125402 (2011).
[15] A. D. Akic, A. B. Djurisic, J. M. Elazar, and M. L. Majewski, Appl. Opt. **37**, 5271 (1998).
[16] CST Studio 2011 online: www.cst.com.
[17] A. Vakil and N. Engheta, Science **332**, 1291 (2011).
[18] I. A. Stegun, *Miscellaneous Functions*, in *Handbook of Mathematical Functions*, edited by I. A. Stegun and M. Abramowitz (Dover, New York, 1970), Chap. 27.